

Localizing Preference Aggregation Conflicts: A Graph-Theoretic Approach Using Sheaves

Karen Sargsyan^{*1}

¹Institute of Chemistry, Academia Sinica, Taipei, Taiwan

December 3, 2025

Abstract

We introduce a graph-theoretic framework based on discrete sheaves to diagnose and localize inconsistencies in preference aggregation. Unlike traditional linearization methods (e.g., HodgeRank), this approach preserves the discrete structure of ordinal preferences, identifying which specific voter interactions cause aggregation failure—information that global methods cannot provide—via the Obstruction Locus. We formalize the Incompatibility Index to quantify these local conflicts and examine their behavior under stochastic variations using the Mallows model. Additionally, we develop a rigorous sheaf-theoretic pushforward operation to model voter merging, implemented via a polynomial-time constraint DAG algorithm. We demonstrate that graph quotients transform distributed edge conflicts into local impossibilities (empty stalks), providing a topological characterization of how aggregation paradoxes persist across scales.

1 Introduction

The challenge of aggregating individual preferences into a collective decision is central to social choice theory. Since the seminal work of Condorcet [1] and the foundational impossibility theorem of Arrow [2], it has been understood that ordinal preference aggregation is inherently susceptible to paradoxes and inconsistencies. These paradoxes typically manifest as cycles (e.g., A preferred over B, B over C, and C over A), obstructing the formation of a coherent global order.

The inherent complexity of this problem has spurred the application of diverse mathematical frameworks, increasingly drawing from topology and geometry to understand the structure of preference spaces and the nature of these obstructions [3, 4]. One prominent approach involves adapting Hodge theory to combinatorial settings, often referred to as “HodgeRank” [5]. This method linearizes the preference data, mapping ordinal comparisons to numerical flows on a graph. While powerful, linearization can obscure the discrete, combinatorial nature of ordinal preferences and may prioritize global topological features over the specific localization of inconsistencies within the profile.

In parallel, sheaf theory has emerged as a powerful mathematical framework for studying local-to-global problems [6–8]. A sheaf provides a formal mechanism to track data assigned to different parts of a space and enforce compatibility on their overlaps. Its application has expanded significantly in applied topology, addressing problems in data fusion, networks, and dynamics [9–11].

This study explores the feasibility of using discrete sheaf theory to analyze preference aggregation without linearization. We propose a computational framework where the data assigned to

^{*}Corresponding author: karen.sarkisyan@gmail.com

vertices (voters) are the preferences themselves—sets of total orders. We introduce the concept of the *Obstruction Locus* (Ω) to rigorously quantify and localize inconsistencies, and demonstrate through computational experiments that this framework reveals interesting phenomena in the structure of preference profiles. Our main contributions are:

1. The definition and implementation of the Discrete Order Sheaf for preference profiles.
2. The rigorous definition of the Obstruction Locus (Ω_1) and the Incompatibility Index ($|\Omega_1|$), with clear explanation of what this quantity measures.
3. Experimental evidence showing how $|\Omega_1|$ varies with profile changes, using both a stochastic interpolation model (demonstrating emergent transitions) and illustrative deterministic examples.
4. Implementation of the rigorous sheaf-theoretic pushforward (π_*), revealing that merging conflicts transforms edge obstructions into local impossibilities (empty stalks).

1.1 Clarification on Scope

We emphasize that the Incompatibility Index $|\Omega_1|$ is *not* a cohomological invariant in the classical sense. Rather, it is the cardinality of the support of the coboundary—essentially, a count of incompatible edges for a given preference profile. The sheaf-theoretic language provides a clean formalization for this localization problem, but readers should not expect the full machinery of sheaf cohomology to be deployed here. Our contribution is primarily computational and conceptual: we show that sheaf-theoretic localization provides information that global linearized methods do not capture.

2 Related Work

The intersection of topology, geometry, and social choice theory is a rich and growing area of research. Our work builds upon several distinct traditions.

2.1 Topological Social Choice

The application of topological methods to social choice was pioneered by Chichilnisky [4], who demonstrated that the topological properties of the space of preferences impose constraints on the existence of continuous aggregation rules satisfying certain axioms (like anonymity and unanimity). This line of research established that contractibility of the domain is often linked to the possibility of aggregation. Subsequent work by Baigent [3] explored preference proximity and its implications for social choice rules. Weinberger [12] extended these concepts to discrete voting schemes, analyzing the topology of voting configurations. Our work builds on this tradition but differs by employing sheaf-theoretic localization specifically to identify which edges in the interaction graph cause inconsistencies.

2.2 Applied Sheaf Theory

Sheaf theory, originally developed in algebraic geometry [6, 7], has recently found significant applications in applied topology. Ghist emphasized the utility of sheaves for understanding distributed systems and sensor networks [10]. Curry provided foundational work on sheaves and cosheaves in applied settings, exploring their connection to persistence and data fusion [9]. Robinson investigated assignments to sheaves of pseudometric spaces, relevant for modeling data with inherent geometric structure [13]. More recently, Hansen and Ghist explored opinion dynamics using discourse sheaves, modeling the evolution of beliefs over networks [11]. Our framework extends these ideas to the domain of ordinal preference aggregation.

2.3 Hodge Theory and Ranking

The adaptation of Hodge theory to discrete settings, particularly for ranking from pairwise comparisons, was formalized by Jiang et al. with HodgeRank [5]. This approach linearizes preference data into flows on a graph and decomposes these flows into gradient flows (consistent rankings) and harmonic flows (inconsistencies or cycles). This provides a robust method for quantifying inconsistency through the L_2 norm of the harmonic component. While effective, Hodge-theoretic methods rely on linearization. As demonstrated in Section 4.1, our discrete, sheaf-theoretic approach reveals localized information about obstructions that linearization obscures.

2.4 Judgment Aggregation and Logical Constraints

Beyond preference aggregation, the broader field of judgment aggregation studies how to combine individual judgments on logically connected propositions [14–16]. The doctrinal paradox and related impossibility results [15] demonstrate that logical constraints between propositions can obstruct consistent aggregation, analogous to how preference cycles obstruct ordinal aggregation. Our sheaf-theoretic framework naturally accommodates such logical constraints through the restriction maps, and the Obstruction Locus can be interpreted as identifying where logical consistency fails across the network.

2.5 Algebraic Approaches to Arrow’s Theorem

Arrow’s theorem has been analyzed through various algebraic lenses [17–19]. The ultrafilter proof of Arrow’s theorem [18] characterizes dictatorships as ultrafilters on the set of voters, providing an elegant algebraic perspective. More recent work by Lauwers and Van Liedekerke [19] connects Arrow’s framework to Boolean algebras. While our approach differs—we focus on localization of conflicts rather than characterization of aggregation rules—these algebraic perspectives inform potential future connections.

2.6 Probabilistic Models of Preferences

The Mallows model [20] provides a probability distribution over permutations centered on a reference ordering, with a dispersion parameter controlling concentration. This model has been proposed in machine learning and statistics for analyzing ranking data [21]. We employ the Mallows model in our stochastic interpolation experiments to generate realistic preference distributions with controllable consensus levels.

3 Framework and Methods

We model a population of voters and their interactions as a graph $G = (V, E)$, where vertices V represent voters and edges E represent interactions (overlaps or shared comparisons) where consistency is required. The set of alternatives over which voters may have preferences is denoted by A .

3.1 The Discrete Order Sheaf

Definition 3.1 (Discrete Order Presheaf). Let F be a presheaf on the graph $G = (V, E)$ with face poset category structure. For each vertex $v \in V$, let $A_v \subseteq A$ denote the subset of alternatives visible at v . We define:

1. **Vertex stalks:** F_v is the set of all total orders on A_v .
2. **Edge stalks:** For each edge $e = \{u, v\} \in E$, let $A_e = A_u \cap A_v$ be the overlap of visible alternatives. Then F_e is the set of all total orders on A_e .

3. **Restriction maps:** For each incidence $v \subseteq e$ (i.e., vertex v incident to edge $e = \{u, v\}$), the restriction map $\rho_e^v : F_v \rightarrow F_e$ is given by:

$$\rho_e^v(\sigma_v) = \sigma_v|_{A_e}$$

where $\sigma_v|_{A_e}$ denotes the restriction of the total order σ_v to the subset $A_e \subseteq A_v$. We denote by $\mathcal{T}(S)$ the set of all total orders on a finite set S .

Lemma 3.1 (Sheaf Property). *The discrete order presheaf F defined above satisfies the sheaf axioms on the face poset of G .*

Proof. For a presheaf on a graph (viewed as a 1-dimensional simplicial complex), the sheaf axioms reduce to checking consistency on edges. For each edge $e = \{u, v\}$:

Locality: Suppose $\sigma_e, \sigma'_e \in F_e$ satisfy $\rho_e^u(\sigma_u) = \sigma_e$ and $\rho_e^u(\sigma'_e) = \sigma'_e$ for some $\sigma_u \in F_u$. Then $\sigma_e = \sigma_u|_{A_e} = \sigma'_e$.

Gluing: Given $\sigma_u \in F_u$ and $\sigma_v \in F_v$ with $\rho_e^u(\sigma_u) = \rho_e^v(\sigma_v)$ (i.e., $\sigma_u|_{A_e} = \sigma_v|_{A_e}$), this common value defines a unique $\sigma_e \in F_e$.

Since graphs have no higher simplices, no further conditions apply. \square

Definition 3.2 (Preference Profile as a 0-Cochain). A preference profile σ is an assignment of a specific local order $\sigma_v \in F_v$ to each vertex v . In the language of the Čech complex, σ is a 0-cochain: $\sigma \in C^0(G, F) = \prod_{v \in V} F_v$.

3.2 The Obstruction Locus (Ω)

We define compatibility constraints using the coboundary operator δ . For an edge $e = \{u, v\}$, the overlap is the intersection of visible alternatives $A_{uv} = A_u \cap A_v$.

Definition 3.3 (Obstruction Locus Ω_1 and Incompatibility Index). The edge Obstruction Locus $\Omega_1(\sigma)$ is the set of edges where local orders are incompatible:

$$\Omega_1(\sigma) = \{e = \{u, v\} \in E \mid \sigma_u|_{A_{uv}} \neq \sigma_v|_{A_{uv}}\}$$

The Incompatibility Index $|\Omega_1(\sigma)|$ is the cardinality of this set.

Remark 3.1 (What $|\Omega_1|$ Measures). *The Incompatibility Index $|\Omega_1(\sigma)|$ counts the number of edges where adjacent voters disagree on their shared alternatives. This is the support of the coboundary $\delta\sigma$, not a cohomological dimension. The key advantage of this measure is localization: it identifies which specific edges cause inconsistency, rather than merely detecting that inconsistency exists.*

Higher-order obstruction loci (e.g., Ω_2) are trivially empty for sheaves of total orders due to transitivity. Algorithmic details for computing Ω_1 are provided in Appendix A.

3.3 Global Consistency (H^0)

Proposition 3.1 (Global Consistency). *A global section exists ($H^0 \neq \emptyset$) if and only if:*

1. *The Obstruction Locus is empty: $\Omega(\sigma) = \emptyset$.*
2. *All stalks are non-empty (local consistency): $F_v \neq \emptyset$ for all $v \in V$.*

Remark 3.2. *Condition (2) is automatically satisfied when each visibility set A_v is nonempty, since total orders exist on any finite nonempty set. However, condition (2) becomes substantive for the pushforward sheaf $\pi_* F^\sigma$, where stalks can become empty due to contradictory constraints.*

3.4 The Rigorous Pushforward (π_*)

Given a graph quotient map $\pi : G \rightarrow G'$ (e.g., a vertex merge), the pushforward sheaf π_*F on G' is defined rigorously.

Definition 3.4 (Rigorous Pushforward Sheaf π_*F^σ). Let $\pi : G \rightarrow G'$ be a graph quotient map (e.g., vertex contraction). Given a preference profile σ on G , we define the pushforward sheaf restricted to σ , denoted π_*F^σ , on G' as follows:

1. **Vertex Stalks:** For a vertex $v' \in V(G')$, let $P = \pi^{-1}(v') \subseteq V(G)$ be its preimage. The set of visible alternatives at v' is $A_{v'} = \bigcup_{v \in P} A_v$. The stalk is the set of total orders on $A_{v'}$ compatible with all original voters in the preimage:

$$(\pi_*F^\sigma)_{v'} = \{\tau \in \mathcal{T}(A_{v'}) \mid \forall v \in P, \tau|_{A_v} = \sigma_v\}$$

where the restriction $\tau|_{A_v}$ denotes the induced order on $A_v \subseteq A_{v'}$.

2. **Edge Stalks:** For an edge $e' = \{u', v'\} \in E(G')$, the stalk is the set of total orders on the overlap $A_{e'} = A_{u'} \cap A_{v'}$ compatible with the incident vertex stalks.

$$(\pi_*F^\sigma)_{e'} = \mathcal{T}(A_{e'})$$

3. **Restriction Maps:** For an incidence $v' \in e'$, the restriction map $r : (\pi_*F^\sigma)_{v'} \rightarrow (\pi_*F^\sigma)_{e'}$ is the standard restriction of a total order to a subset of alternatives.

If the constraints in the preimage P are contradictory (e.g., forming a cycle in the constraint DAG), the vertex stalk $(\pi_*F^\sigma)_{v'}$ becomes the empty set \emptyset . Consequently, any restriction map originating from this empty stalk has an empty image, propagating the local impossibility to incident edges.

3.4.1 Computational Method: Constraint DAG Approach

Computing the pushforward stalk efficiently requires determining which total orders on the full set of alternatives A are compatible with all local orders in the preimage. A naive approach would enumerate all $|A|!$ permutations, which is exponential and infeasible for large $|A|$. Instead, we employ a constraint directed acyclic graph (DAG) approach. The key insight is that each local order in the preimage imposes pairwise ordering constraints. For a voter with order $a_1 > a_2 > \dots > a_k$, we have constraints $a_i > a_{i+1}$ for all i . Compatibility requires that any global order respects all such constraints from all voters in the preimage.

Algorithm Overview:

1. **Build constraint DAG C :** Create a directed graph with vertices = alternatives A and add edge (a, b) for each pairwise constraint “ a must precede b ” from any voter in the preimage.
2. **Detect cycles:** If C contains a directed cycle, the constraints are contradictory and the stalk is empty. This occurs when voters have conflicting preferences (e.g., V_1 requires $A > B$ while V_2 requires $B > A$).
3. **Find compatible orders:** If C is acyclic (a DAG), any topological ordering of C yields a compatible total order. The set of all topological orderings constitutes the pushforward stalk.

This approach reduces the complexity from $O(|A|!)$ to $O(|A|^2 \cdot |P|)$ for cycle detection, where $|P|$ is the size of the preimage. Building the DAG requires $O(|A| \cdot |P|)$ time (adding edges for each voter’s constraints), and cycle detection via depth-first search is $O(|A| + |E_C|)$ where $|E_C| \leq |A|^2$ is the number of constraint edges.

Remark 3.3 (DAG as Intersection of Constraints). *The definition of the pushforward stalk $(\pi_* F^\sigma)_{v'}$ requires finding an order τ that satisfies multiple local conditions simultaneously. In set-theoretic terms, the stalk is the intersection of the solution sets of individual voters. The constraint DAG algorithm computes this intersection efficiently. A cycle in the DAG corresponds to an empty intersection ($\bigcap \text{valid orders} = \emptyset$), providing a computational certificate that the stalk is empty.*

Remark 3.4 (Empty Stalk Detection). *A cycle in the constraint DAG immediately certifies that the pushforward stalk is empty. For example, if merging voters V_1 with order $A > B > C$ and V_2 with order $B > C > A$, the constraints form a cycle $A \rightarrow B \rightarrow C \rightarrow A$, proving no compatible order exists.*

Remark 3.5 (Enumeration Complexity). *While cycle detection is polynomial, enumerating all compatible total orders is $\#P$ -complete in the worst case, as it requires counting all linear extensions of the constraint DAG. For most practical preference profiles, the constraint DAG is highly constrained, yielding few compatible orders. Our implementation returns one witness ordering for large $|A|$, which suffices for existence proofs and empty stalk detection.*

The complete algorithm with complexity analysis appears in Appendix A; a worked example demonstrating empty stalk detection is provided in Appendix B.

3.5 Stochastic Model: Mallows Distribution

To study how $|\Omega_1|$ varies with preference distributions, we employ the Mallows model [20], a probability distribution over permutations.

Definition 3.5 (Mallows Model). Given a reference permutation π_0 and dispersion parameter $\phi \in (0, 1]$, the Mallows model assigns probability:

$$P(\pi \mid \pi_0, \phi) \propto \phi^{d(\pi, \pi_0)}$$

where $d(\pi, \pi_0)$ is the Kendall tau distance (number of pairwise inversions) between π and π_0 .

When $\phi \rightarrow 0$, the distribution concentrates on π_0 . When $\phi = 1$, the distribution is uniform over all permutations. This allows us to interpolate smoothly between consensus (ϕ small) and maximum diversity ($\phi = 1$).

4 Computational Experiments

In this section, we analyze several examples to demonstrate the capabilities of our framework. All results were obtained using Python implementations within the Discrete Order Sheaf framework. Basic examples validate the framework’s ability to detect known paradoxes (Table 1).

Table 1: Obstruction Loci of Discrete Order Sheaves: Computational Results for Basic Examples. Detailed configurations for Partial Visibility and K_4 are provided in Appendix D.

Example	H^0 exists	$ \Omega_1 $	$ \Omega_2 $	Notes
Condorcet Triangle	False	3	0	All 3 edges incompatible
Transitive Triangle	True	0	0	Unanimous agreement
Partial Visibility	False	1	0	Single conflicting edge
Complete K_4	False	5	0	Edge (V_1, V_4) compatible*

*In the K_4 example, voters V_1 and V_4 both have order $A > B > C$, making their shared edge compatible. The remaining 5 edges connect voters with distinct cyclic orderings.

4.1 Localization and the Role of Topology

4.1.1 Discrete vs. Linearized Obstructions

We compared the Incompatibility Index $|\Omega_1|$ with the dimension of the linearized cohomology group H_{lin}^1 [5]. We analyzed the standard Condorcet profile on a triangle (K_3). The discrete framework yields $|\Omega_1| = 3$, identifying that all three edges are incompatible. In contrast, H_{lin}^1 measures the cycle rank of the underlying graph ($E - V + C = 1$). As illustrated in Figure 1, the Obstruction Locus provides localized information that linearized cohomology does not capture: the linearized version detects global inconsistency but does not indicate which edges are responsible.

Why linearization loses localization: HodgeRank embeds orderings into $\mathbb{R}^{|A|}$ and measures inconsistency via the L_2 norm of the harmonic flow. This projection loses the discrete identity of individual orderings—two profiles with different obstruction loci can have identical harmonic norms. Our discrete approach preserves this edge-level information.

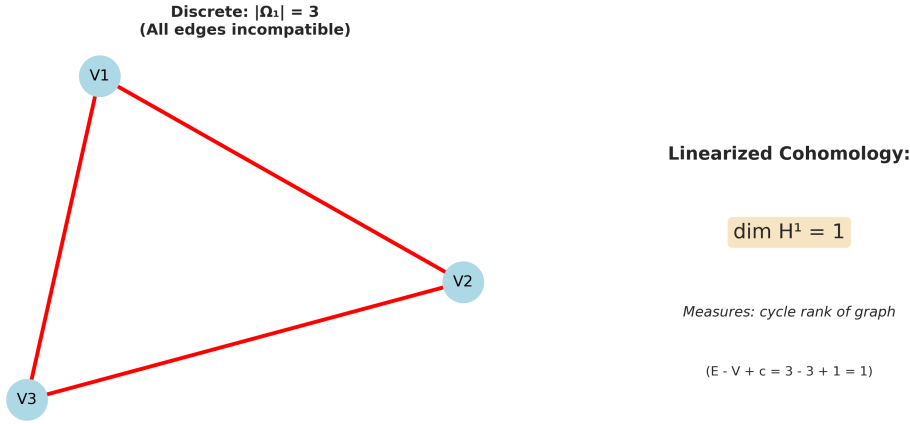


Figure 1: Comparison between the Discrete Obstruction Locus and Linearized Cohomology for a Condorcet cycle. The discrete approach identifies *all three edges* as incompatible ($|\Omega_1| = 3$), pinpointing where coalition formation fails. Linearized cohomology yields only the cycle rank ($\dim H_{\text{lin}}^1 = 1$), which would be identical for *any* cyclic graph regardless of which edges carry conflicts.

4.1.2 Consistency of Random Preferences

We simulated random preference profiles (over three alternatives) on various graph structures (N=100 trials each; see Appendix D for topology definitions). We measured two statistical metrics:

1. **Consistency Rate:** The proportion of trials where a global section exists ($H^0 \neq \emptyset$). This measures the probability of spontaneous consensus.
2. **Average Incompatibility Index:** The mean value of $|\Omega_1|$ across all trials. This quantifies the expected number of conflicting interactions.

Theoretical baseline: For $|A| = 3$ alternatives, the probability that two random voters agree on their shared ranking is $1/3! = 1/6$. Consequently, an edge is obstructed with probability $5/6$. On a triangle graph (K_3), the condition for global consistency requires agreement on two edges (which implies the third by transitivity), yielding a theoretical consistency rate of $(1/6)^2 \approx 2.8\%$.

Our observed consistency rate of $\sim 3\%$ for K_3 matches this theoretical expectation (Figure 2), validating the framework. The results show that highly connected graphs (e.g., K_4) exhibit near-zero consistency rates and high average $|\Omega_1|$, reflecting the "cost of connectivity": each additional interaction introduces a new potential locus for conflict. The results (Figure 2) show consistency rates and average obstruction counts across different topologies.

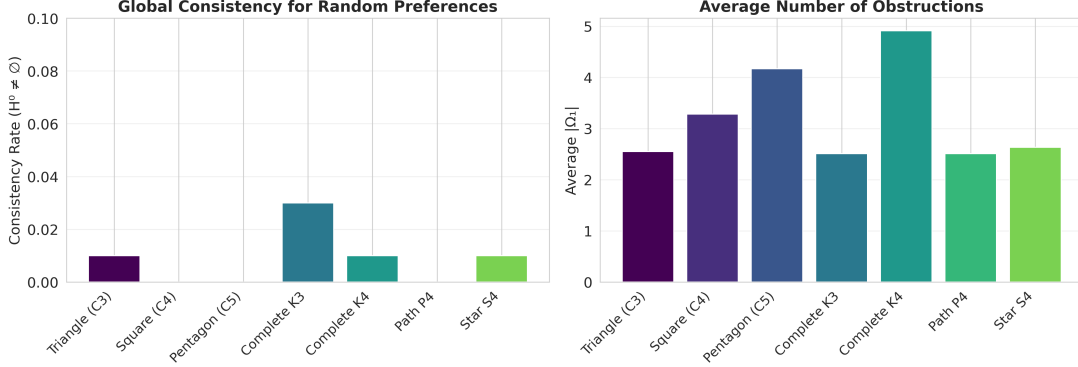


Figure 2: Global consistency rates and average Incompatibility Index for random preference profiles on different graph topologies. Consistency rates match theoretical expectations (e.g., $\sim 2.8\%$ for K_3 with uniform random preferences).

4.2 Variation of the Obstruction Locus

We investigate how the Obstruction Locus changes as preference profiles vary. We present two complementary experiments: (1) a stochastic interpolation using Mallows distributions that demonstrates emergent transitions, and (2) an illustrative deterministic family that serves as scaffolding to show how $|\Omega_1|$ responds to discrete preference changes.

4.2.1 Stochastic Interpolation via Mallows Model

To demonstrate how $|\Omega_1|$ varies with preference distributions, we constructed a stochastic interpolation model. We consider three voters on a triangle graph, where each voter’s preferences are drawn from Mallows distributions.

Model setup: At parameter $t = 0$, each voter has a distinct reference ordering that together form a Condorcet cycle: V_1 prefers $A > B > C$, V_2 prefers $B > C > A$, and V_3 prefers $C > A > B$. As t increases toward 1, voters’ reference orderings gradually shift toward a common consensus ($A > B > C$), and the dispersion parameter ϕ decreases (concentrating preferences near their references).

Interpolation scheme: The reference ordering for each voter V_i transitions deterministically: V_2 ’s reference changes from $B > C > A$ to $A > B > C$ at $t = 0.5$, and V_3 ’s reference changes from $C > A > B$ to $A > B > C$ at $t = 0.75$. The dispersion parameter follows $\phi(t) = 0.8 - 0.5t$, so that $\phi(0) = 0.8$ (high diversity) and $\phi(1) = 0.3$ (concentrated near consensus). Crucially, the observed transitions in $|\Omega_1|$ emerge from the probabilistic sampling, not from the discrete reference switches—intermediate t values exhibit smooth behavior due to the stochastic draws from Mallows distributions.

We sample $N = 500$ profiles at each parameter value and compute the distribution of $|\Omega_1|$.

Results (Figure 3):

1. The mean $|\Omega_1|$ transitions smoothly from 2.48 ± 0.65 at $t = 0$ to 0.97 ± 1.10 at $t = 1$.
2. The standard deviation is highest at intermediate t values, reflecting the stochastic nature of the transition.

3. The consistency rate (probability that H^0 exists) increases monotonically from 2.8% to 55.2%.
4. The distribution of $|\Omega_1|$ values shifts continuously from being concentrated at high values (2-3) to low values (0-1).

These results demonstrate that the Obstruction Locus captures meaningful structural information about preference distributions and responds predictably to changes in consensus levels.

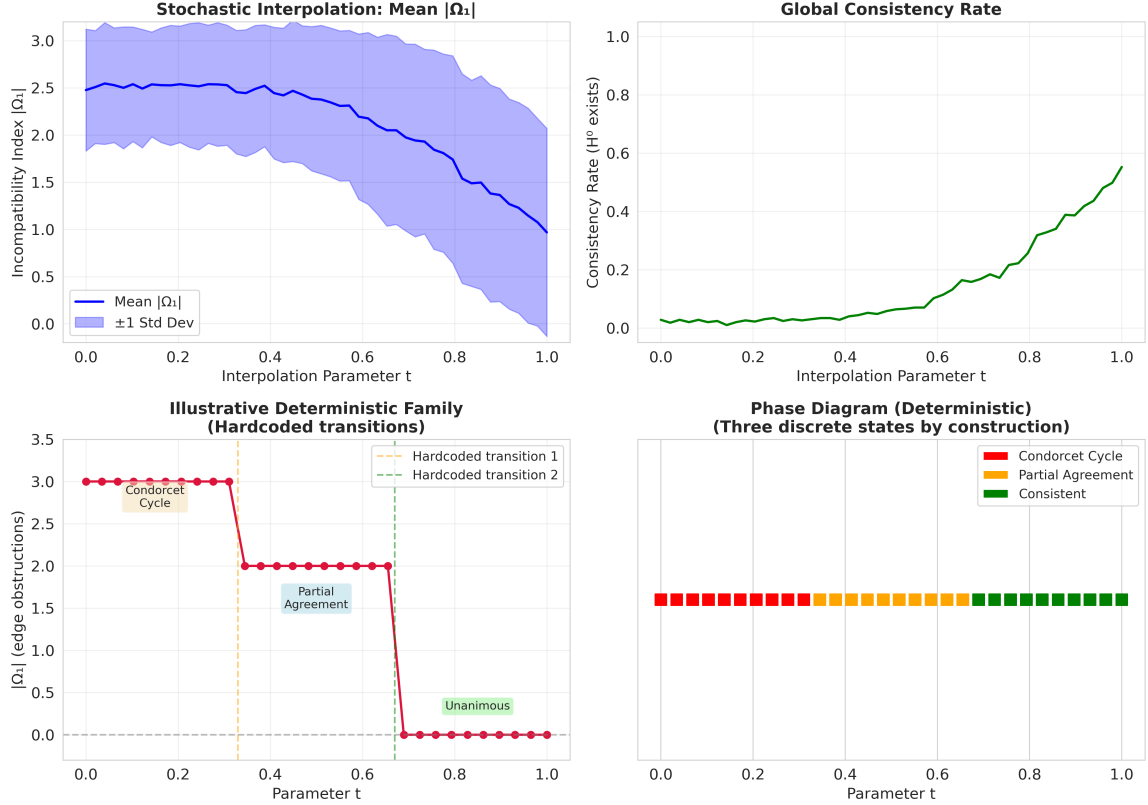


Figure 3: Stochastic interpolation via Mallows model. (Top left) Mean $|\Omega_1|$ with standard deviation band shows smooth emergent transition. (Top right) Consistency rate increases monotonically. (Bottom) Illustrative deterministic family showing $|\Omega_1|$ transitions.

4.2.2 Illustrative Deterministic Family

To illustrate the framework’s sensitivity to preference changes, we also constructed a deterministic parametric family $\{F_t\}_{t \in [0,1]}$ with hardcoded transitions at $t = 1/3$ and $t = 2/3$, where voters switch their preferences according to a predefined schedule.

Important caveat: This experiment is illustrative scaffolding, not evidence of emergent phenomena. The discrete jumps in $|\Omega_1|$ at $t = 1/3$ and $t = 2/3$ occur by design—we explicitly programmed voters to change their preferences at these points. The experiment serves only to verify that our computational framework correctly detects these changes and to provide a visual contrast with the emergent stochastic behavior.

The results (Figure 3) show $|\Omega_1|$ dropping from 3 to 2 at $t = 1/3$, and from 2 to 0 at $t = 2/3$, exactly as constructed. This validates the framework’s sensitivity.

4.3 The Rigorous Pushforward under Quotient

Let us examine the behavior of the sheaf under a graph quotient map π . We start with a Condorcet cycle (V_1, V_2, V_3) , where $|\Omega_1| = 3$, and merge V_1 and V_2 into V_{12} (Figure 4). Then

we apply the rigorous pushforward π_*F using the constraint DAG method described in Section 3.4.

To compute the stalk $(\pi_*F)_{V12}$, we build a constraint DAG from the orders of V1 ($A > B > C$) and V2 ($B > C > A$):

- V1 imposes: $A \rightarrow B, B \rightarrow C$
- V2 imposes: $B \rightarrow C, C \rightarrow A$

The resulting DAG contains edges $A \rightarrow B \rightarrow C \rightarrow A$, forming a directed cycle. This cycle immediately certifies that no total order can satisfy both constraints, proving that the stalk $(\pi_*F)_{V12}$ is *empty*. See Appendix C for the formal proof and Appendix B for the complete DAG construction.

The Incompatibility Index on the quotient graph drops to $|\Omega_1| = 0$, as the empty stalk is vacuously compatible with V3. However, H^0 remains empty due to the local impossibility at V12. The obstruction transformed from edge incompatibilities into the structure of the stalk itself. Importantly, this empty stalk phenomenon is verified computationally via the constraint DAG cycle, not merely proven abstractly.

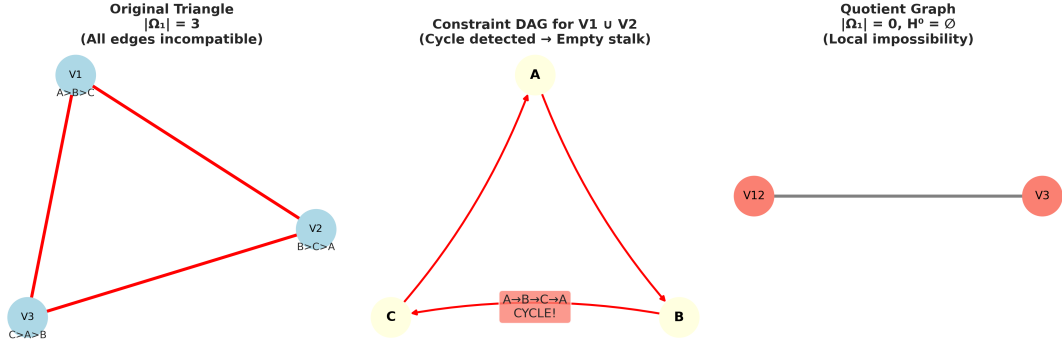


Figure 4: Rigorous Pushforward under Quotient. Merging conflicting voters V1 and V2 results in an empty stalk at V12. The obstruction persists as a local impossibility.

4.4 Scaling Experiments

To validate the practical efficiency of the DAG-based pushforward algorithm, we conducted scaling experiments measuring runtime and memory usage across different problem sizes.

4.4.1 Scaling with Number of Alternatives

We tested the cycle detection algorithm for $|A| \in \{6, 8, 10, 12\}$ alternatives with $|P| = 5$ voters in the merge preimage (Table 2). For $|A| \leq 8$, we measured naive enumeration time directly; for larger $|A|$, naive times are extrapolated since direct measurement is infeasible.

Table 2: Complexity Comparison: DAG vs Naive Enumeration

$ A $	$ A !$	DAG (ms)	Naive (ms)	Speedup	Memory (KB)
6	720	0.53	0.20	$< 1\times$	18.9
8	40,320	0.75	13.6	$18\times$	20.9
10	3,628,800	0.97	1,222*	$1,263\times$	25.3
12	479,001,600	1.08	161,316*	$149,300\times$	30.1

*Estimated by extrapolation from $|A| = 8$. Timing averaged over 50 trials, $|P| = 5$ voters.

For small $|A| = 6$, the overhead of building the DAG exceeds the naive enumeration time. However, the crossover occurs around $|A| = 7$, after which the DAG approach dominates. At $|A| = 12$, the speedup exceeds $149,000\times$ —naive enumeration would require approximately 2.7 minutes versus ~ 1 ms for DAG cycle detection.

Memory usage scales modestly: from 18.9 KB at $|A| = 6$ to 30.1 KB at $|A| = 12$, reflecting the $O(|A|^2)$ edge storage in the constraint DAG.

4.4.2 Realistic Scenario: Committee Decision

We simulated a realistic preference aggregation scenario with $|V| = 50$ voters and $|A| = 8$ alternatives on a random graph (Erdős-Rényi, $p = 0.15$, yielding 179 edges). Computing Ω_1 over all edges required 0.15 ms. The incompatibility rate was 97.2% (174 of 179 edges), reflecting a high-conflict scenario with diverse preferences.

For pushforward computation, we merged 5 randomly selected voters. Cycle detection completed in 1.9 ms with 26.0 KB memory, confirming an empty stalk via the cycle $(0 \rightarrow 2 \rightarrow 1 \rightarrow 0)$. This demonstrates that the framework handles realistic problem sizes with sub-millisecond to single-digit millisecond response times.

4.4.3 Scaling with Merge Size

We also tested how cycle detection time scales with the number of voters being merged ($|P|$), holding $|A| = 8$ fixed. Runtime increased from 0.34 ms at $|P| = 3$ to 15.5 ms at $|P| = 50$, consistent with the $O(|A|^2 \cdot |P|)$ complexity bound.

Notably, the conflict rate was 100% across all merge sizes when using uniformly random preferences—random voters almost always have conflicting constraints, resulting in empty stalks. This underscores the practical importance of efficient empty stalk detection.

5 Discussion

The computational framework presented here establishes a foundation for analyzing social choice obstructions using discrete sheaf theory. By focusing on localization of incompatibilities, we have developed metrics and tools that accurately reflect the structure of aggregation paradoxes.

5.1 Interpretation of Results

The distinction between the Incompatibility Index $|\Omega_1|$ and the linearized cohomology H_{lin}^1 is significant (cf. Remark 3.1). While H_{lin}^1 measures global topological features [5], $|\Omega_1|$ identifies the specific edges where coherence fails. This localization is crucial for understanding how specific interactions contribute to global impossibilities.

The stochastic interpolation experiment (Section 4.2.1) demonstrates that $|\Omega_1|$ responds smoothly to changes in preference distributions. The emergent nature of these transitions—arising from the Mallows model rather than hardcoded rules—provides evidence that the Obstruction Locus captures meaningful structural information about preference profiles.

The most significant experimental finding is the behavior of the rigorous pushforward (π_*) . The empty stalk phenomenon reveals a fundamental principle: aggregation conflicts cannot be resolved by simple merging or coarse-graining without information loss or the imposition of an aggregation rule. The pushforward functor naturally captures this impossibility by transforming distributed conflicts (edge obstructions) into localized impossibilities (empty stalks). This demonstrates the capacity of the sheaf-theoretic framework to track obstructions across different scales of analysis.

5.2 Connection to Classical Social Choice Theory

This framework offers a new lens through which to view classical results.

5.2.1 Domain Restrictions

Classical social choice theory identifies specific restrictions on the domain of preferences that guarantee consistent aggregation, such as single-peaked preferences [22]. Single-peakedness typically implies an underlying linear structure. In our model, such preferences often correspond to profiles defined on acyclic graphs (like paths or trees). Our experiments (Figure 2) suggest that acyclic graphs have higher consistency rates. The sheaf framework allows for the precise study of how domain restrictions relate to the vanishing of the Obstruction Locus ($\Omega = 0$).

5.2.2 Connection to Judgment Aggregation

The framework naturally extends to judgment aggregation settings [14, 15]. In judgment aggregation, individuals hold positions on logically connected propositions, and the challenge is to aggregate these into a consistent collective judgment. The Obstruction Locus can identify which logical constraints are violated when aggregating, providing localized diagnostics analogous to our preference setting.

5.3 Computational Complexity

The computational tractability of this framework is crucial for practical applications.

5.3.1 Computing the Obstruction Locus

Computing the Obstruction Locus Ω_1 involves checking compatibility on every edge. If $|A|$ is the number of alternatives, determining the restriction on an overlap takes $O(|A|)$ time. Thus, the total complexity for computing Ω_1 is $O(|E| \cdot |A|)$, which is polynomial and efficient (Appendix A).

5.3.2 Computing the Rigorous Pushforward

The pushforward computation has been optimized using a constraint DAG approach. The key operations are:

1. Build a constraint DAG from pairwise ordering requirements: $O(|A| \cdot |P|)$
2. Detect cycles via depth-first search: $O(|A| + |E_C|)$ where $|E_C| \leq |A|^2$
3. If acyclic, find topological orderings: $O(|A| + |E_C|)$ for one ordering

The total complexity for cycle detection (empty stalk verification) is $O(|A| \cdot |P| + |E_C|)$ where $|E_C| \leq |A| \cdot |P|$ is the number of constraint edges, which simplifies to $O(|A| \cdot |P|)$. The bound $O(|A|^2 \cdot |P|)$ stated in Section 3.4 is conservative, accounting for the case where constraint edges approach $|A|^2$ (which occurs only with many voters having diverse preferences).

Table 3: Pushforward Complexity Comparison

Approach	Complexity	Feasible for $ A $
Naive (factorial)	$O(A ! \cdot P)$	≤ 8
DAG (cycle detection)	$O(A ^2 \cdot P)$	$\leq 100+$
DAG (enumerate all)	#P-complete	varies

Caveat on enumeration: While cycle detection is polynomial, enumerating *all* compatible orders is $\#P$ -complete in the worst case, as it requires counting linear extensions of the constraint DAG. For empty stalk detection and existence proofs, cycle detection suffices. Our implementation returns one witness ordering for large $|A|$, which is practical for most applications.

For $|A| = 10$ alternatives and $|P| = 3$ voters:

- Naive: $10! \cdot 3 \approx 10.9$ million operations
- DAG (cycle detection): ~ 300 operations

This dramatic speedup makes the pushforward computation practical for real-world applications where detecting impossibility (empty stalks) is the primary goal.

5.4 Limitations and Future Directions

Several limitations warrant discussion:

Triviality of higher obstructions. The higher-order obstruction loci ($\Omega_k, k \geq 2$) are trivially empty when using total orders, due to transitivity. To capture meaningful higher-dimensional obstructions, the framework would need to be generalized to sheaves of *partial orders* or *interval orders*.

Graph selection. The framework assumes a known, fixed interaction graph G . In practice, the choice of G —which voter pairs are required to be consistent—is a modeling decision that significantly affects results. Future work should address principled methods for constructing G from data.

Scalability. While our algorithms are polynomial, computing Ω_1 for very large graphs ($|V| \gg 1000$) with many alternatives may require parallelization or approximation schemes.

Future directions. Connecting this framework to **persistent homology** [23] could enable analysis of how preference profiles evolve over time or across different scales of interaction. Additionally, extending to weighted graphs (where edges have varying importance) would increase practical applicability.

6 Conclusion

We have introduced a computational framework for analyzing discrete preference aggregation using sheaf theory. By rigorously defining the Obstruction Locus (Ω), we provide a tool to localize and quantify the impediments to global consistency. Our experiments demonstrate that $|\Omega_1|$ varies smoothly with preference distributions (via stochastic interpolation using Mallows models) and that the rigorous pushforward transforms edge conflicts into local impossibilities (empty stalks). The polynomial-time pushforward algorithm, based on constraint DAG cycle detection, makes these methods practical for real-world applications.

The sheaf-theoretic language provides a clean framework for this localization problem, enabling precise definitions and the pushforward construction. We hope this framework proves useful for analyzing preference aggregation in settings where knowing where conflicts occur matters as much as knowing that they occur.

Availability of Data and Materials

The computational suite implemented for this study, including all code and generated data, is available upon request.

Competing Interests

The authors declare no competing interests.

A Algorithmic Details

A.1 Computing the Obstruction Locus (Ω_1)

The Obstruction Locus $\Omega_1(\sigma)$ is computed by iterating over all edges and checking the compatibility of the restricted local orders.

Algorithm 1 Compute $\Omega_1(\sigma)$

Require: Graph $G = (V, E)$, Preference profile σ , Visibility sets $\{A_v\}_{v \in V}$

Ensure: Obstruction locus Ω_1

```

1:  $\Omega_1 \leftarrow \emptyset$ 
2: for each edge  $e = \{u, v\} \in E$  do
3:    $A_{uv} \leftarrow A_u \cap A_v$  ▷ Compute overlap
4:   if  $|A_{uv}| \geq 2$  then
5:      $\sigma_u^e \leftarrow$  restriction of  $\sigma_u$  to  $A_{uv}$ 
6:      $\sigma_v^e \leftarrow$  restriction of  $\sigma_v$  to  $A_{uv}$ 
7:     if  $\sigma_u^e \neq \sigma_v^e$  then
8:        $\Omega_1 \leftarrow \Omega_1 \cup \{e\}$  ▷ Incompatible edge found
9:     end if
10:  end if
11: end for return  $\Omega_1$ 

```

Complexity: $O(|E| \cdot |A|)$.

A.2 Rigorous Pushforward Computation via Constraint DAG

Given a quotient map $\pi : G \rightarrow G'$, we compute the stalk of the pushforward sheaf $(\pi_* F)_{v'}$ at a vertex $v' \in G'$ using a polynomial-time constraint DAG approach.

Algorithm 2 Compute Stalk of Pushforward $(\pi_*F)_{v'}$ (DAG Method)

Require: Quotient map π , Vertex $v' \in G'$, Profile σ on G , Alternatives A

Ensure: Stalk $S_{v'}$ (Set of compatible orders, or \emptyset if empty)

```

1:  $P \leftarrow \pi^{-1}(v')$  ▷ Identify preimage in G
2: Initialize directed graph  $C$  with vertices  $A$  and no edges ▷ Constraint DAG
3:
4: for each  $v \in P$  do ▷ Build constraint DAG
5:    $\sigma_v \leftarrow$  local order at vertex  $v$ 
6:    $A_v \leftarrow$  visibility set at  $v$ 
7:   for each consecutive pair  $(a_i, a_{i+1})$  in  $\sigma_v$  do
8:     Add directed edge  $a_i \rightarrow a_{i+1}$  to  $C$  ▷ Pairwise constraint
9:   end for
10: end for
11:
12: if  $C$  contains a directed cycle then ▷ Detect contradictory constraints
13:   return  $\emptyset$  ▷ Empty stalk (local impossibility)
14: else
15:    $S_{v'} \leftarrow \{\text{all topological orderings of } C\}$  ▷ All compatible orders
16:   return  $S_{v'}$ 
17: end if

```

Complexity:

- **DAG construction:** $O(|A| \cdot |P|)$ — Each voter contributes $O(|A|)$ edges
- **Cycle detection:** $O(|A| + |E_C|)$ — Depth-first search, where $|E_C| \leq |A|^2$
- **Total:** $O(|A|^2 \cdot |P|)$ — Polynomial in both $|A|$ and $|P|$

This is a dramatic improvement over the naive $O(|A|! \cdot |P|)$ factorial approach.

Remark A.1 (Enumeration of Compatible Orders). *If the constraint DAG is acyclic, the number of compatible orders equals the number of linear extensions of C . Counting these is $\#P$ -complete in general, but cycle detection alone suffices for empty stalk verification.*

B Worked Example: Pushforward Computation via DAG

Consider the Condorcet triangle on G with alternatives $A = \{A, B, C\}$:

$$\begin{aligned}
 \sigma_{V1} &: A > B > C \\
 \sigma_{V2} &: B > C > A \\
 \sigma_{V3} &: C > A > B
 \end{aligned}$$

We apply the quotient map $\pi : G \rightarrow G'$ that merges $V1$ and $V2$ into $V12$. The preimage is $P = \{V1, V2\}$.

Step 1: Build Constraint DAG

We create a directed graph C with vertices $\{A, B, C\}$ and add edges based on each voter's constraints:

From $V1$ ($A > B > C$):

- Add edge $A \rightarrow B$ (A must precede B)

- Add edge $B \rightarrow C$ (B must precede C)

From V2 ($B > C > A$):

- Add edge $B \rightarrow C$ (already present)
- Add edge $C \rightarrow A$ (C must precede A)

Resulting DAG C: Edges are $\{A \rightarrow B, B \rightarrow C, C \rightarrow A\}$.

Step 2: Detect Cycles

The path $A \rightarrow B \rightarrow C \rightarrow A$ forms a directed cycle. This immediately proves:

The stalk $(\pi_* F)_{V_{12}}$ is EMPTY.

Step 3: Interpretation

The cycle $A \rightarrow B \rightarrow C \rightarrow A$ encodes the logical contradiction:

- V1 requires: A before B before C
- V2 requires: C before A
- Combined: A before B before C before A (impossible!)

No total order on $\{A, B, C\}$ can simultaneously satisfy both V1's and V2's preferences. The constraint DAG makes this contradiction explicit and verifiable in polynomial time.

Comparison with Naive Approach

For completeness, we verify by enumeration. We check all $3! = 6$ permutations of A :

1. $\tau = (A, B, C)$: Compatible with V1 (\checkmark), Incompatible with V2 (\times).
2. $\tau = (A, C, B)$: Incompatible with V1 (\times).
3. $\tau = (B, A, C)$: Incompatible with V1 (\times).
4. $\tau = (B, C, A)$: Incompatible with V1 (\times), Compatible with V2 (\checkmark).
5. $\tau = (C, A, B)$: Incompatible with V1 (\times).
6. $\tau = (C, B, A)$: Incompatible with V1 (\times).

Since no total order τ is compatible with both V1 and V2 simultaneously, the stalk $(\pi_* F)_{V_{12}}$ is empty. This matches the DAG result but required checking 6 orderings. For $|A| = 10$, the naive approach would require checking $10! = 3,628,800$ orderings, while the DAG approach needs only cycle detection ($O(|A|^2) = 100$ operations).

C Proofs

Proposition C.1. *Let $\pi : G \rightarrow G'$ be a quotient map merging vertices $V_1, V_2 \in G$ into $v' \in G'$. If the local orders σ_{V_1} and σ_{V_2} are conflicting (incompatible) on their overlap $A_{12} = A_1 \cap A_2$, then the stalk of the pushforward sheaf $(\pi_* F)_{v'}$ is empty.*

Proof. By definition of the pushforward, the stalk $(\pi_* F)_{v'}$ consists of sections τ defined over the preimage $\pi^{-1}(v')$ that are compatible with the local sections in the preimage.

Compatibility requires that the restriction of τ to the domain of each local section matches that section. Specifically for V_1 and V_2 :

$$\tau|_{A_1} = \sigma_{V_1} \tag{1}$$

$$\tau|_{A_2} = \sigma_{V_2} \tag{2}$$

Consider the overlap A_{12} . We restrict equations (1) and (2) further to A_{12} :

$$(\tau|_{A_1})|_{A_{12}} = \sigma_{V_1}|_{A_{12}} \tag{3}$$

$$(\tau|_{A_2})|_{A_{12}} = \sigma_{V_2}|_{A_{12}} \tag{4}$$

Since restriction operations commute (i.e., $(\tau|_{A_1})|_{A_{12}} = \tau|_{A_{12}}$), we must have:

$$\tau|_{A_{12}} = \sigma_{V_1}|_{A_{12}} \quad \text{and} \quad \tau|_{A_{12}} = \sigma_{V_2}|_{A_{12}}$$

This implies that $\sigma_{V_1}|_{A_{12}} = \sigma_{V_2}|_{A_{12}}$.

However, the hypothesis states that the local orders are conflicting on their overlap, meaning $\sigma_{V_1}|_{A_{12}} \neq \sigma_{V_2}|_{A_{12}}$. This is a contradiction.

Therefore, no such compatible section τ exists, and the stalk $(\pi_* F)_{v'}$ must be empty. \square

D Configuration of Validation Examples and Experiments

To ensure reproducibility, we provide the exact graph topologies, visibility sets, and preference assignments used in Section 4.

D.1 Basic Validation Examples

The results reported in Table 1 correspond to the following specific configurations.

Partial Visibility Example ($|\Omega_1| = 1$) This example demonstrates that obstructions can arise solely from the restriction to shared alternatives, even if the graph has cycles.

- **Graph:** Cycle graph C_3 (Triangle) with vertices $V = \{V_1, V_2, V_3\}$.
- **Alternatives:** $A_{\text{global}} = \{A, B, C, D\}$.
- **Visibility Sets:**
 - V_1 sees $\{A, B, C\}$
 - V_2 sees $\{B, C, D\}$
 - V_3 sees $\{A, C, D\}$
- **Preferences (Orders):**
 - $\sigma_{V_1} : A > B > C$
 - $\sigma_{V_2} : B > C > D$

– $\sigma_{V_3} : C > D > A$

- **Analysis:**

- Edge (V_1, V_2) : Overlap $\{B, C\}$. V_1 implies $B > C$; V_2 implies $B > C$. **Compatible.**
- Edge (V_2, V_3) : Overlap $\{C, D\}$. V_2 implies $C > D$; V_3 implies $C > D$. **Compatible.**
- Edge (V_3, V_1) : Overlap $\{A, C\}$. V_1 implies $A > C$; V_3 implies $C > A$. **Incompatible.**

- **Result:** Total $|\Omega_1| = 1$.

Complete K_4 Example ($|\Omega_1| = 5$) This example represents a "Condorcet + 1 Consensus" configuration on a tetrahedron.

- **Graph:** Complete graph K_4 (4 vertices, 6 edges).

- **Alternatives:** $\{A, B, C\}$ visible to all.

- **Preferences:**

- $\sigma_{V_1} : A > B > C$
- $\sigma_{V_2} : B > C > A$
- $\sigma_{V_3} : C > A > B$
- $\sigma_{V_4} : A > B > C$ (Identical to V_1)

- **Analysis:** Vertices V_1, V_2, V_3 form a Condorcet cycle (3 conflicting edges). Vertex V_4 agrees perfectly with V_1 (edge $V_1 - V_4$ is compatible), but inherits V_1 's conflicts with V_2 and V_3 (2 conflicting edges).

- **Result:** Total $|\Omega_1| = 3 + 0 + 2 = 5$.

D.2 Topologies for Random Preference Experiments

In Section 4.1.2 (Figure 2), we evaluated consistency rates on the following graph topologies. In all cases, the set of alternatives was $A = \{A, B, C\}$ and preferences were drawn uniformly at random from the $3! = 6$ possible permutations.

Topology	Nodes ($ V $)	Edges ($ E $)	Description
Triangle (C_3)	3	3	Cycle graph
Square (C_4)	4	4	Cycle graph
Pentagon (C_5)	5	5	Cycle graph
Complete K_3	3	3	Equivalent to C_3
Complete K_4	4	6	Tetrahedron
Path P_4	4	3	Linear chain (1 – 2 – 3 – 4)
Star S_4	4	3	Central hub connected to 3 leaves

Table 4: Graph topologies used for random preference scaling experiments.

References

- [1] De Condorcet, N. (2014). *Essai sur l'application de l'analyse à la probabilité des décisions rendues à la pluralité des voix*. Cambridge University Press. (Original work published 1785)
- [2] Arrow, K. J. (1951). *Social Choice and Individual Values*. Wiley.
- [3] Baigent, N. (1987). Preference proximity and anonymous social choice. *Quarterly Journal of Economics*, 102(1), 161-170.
- [4] Chichilnisky, G. (1980). Social choice and the topology of spaces of preferences. *Advances in Mathematics*, 37(2), 165-176.
- [5] Jiang, X., Lim, L.-H., Yao, Y., & Ye, Y. (2011). Statistical ranking and combinatorial Hodge theory. *Mathematical Programming*, 127(1), 203-244.
- [6] Bredon, G. E. (1997). *Sheaf Theory* (2nd ed.). Springer.
- [7] Kashiwara, M., & Schapira, P. (2006). *Categories and Sheaves*. Springer.
- [8] Rosiak, D. (2022). *Sheaf Theory Through Examples*. MIT Press.
- [9] Curry, J. (2014). Sheaves, cosheaves and applications. PhD thesis, University of Pennsylvania.
- [10] Ghrist, R. (2014). *Elementary Applied Topology*. Createspace.
- [11] Hansen, J., & Ghrist, R. (2019). Opinion dynamics on discourse sheaves. arXiv:1907.04285.
- [12] Weinberger, S. (2004). On the topological social choice model. *Journal of Economic Theory*, 115, 377-384.
- [13] Robinson, M. (2017). Assignments to sheaves of pseudometric spaces. arXiv:1705.07645.
- [14] List, C. (2002). Two concepts of agreement. *The Good Society*, 11(1), 72-79.
- [15] List, C., & Pettit, P. (2002). Aggregating sets of judgments: An impossibility result. *Economics and Philosophy*, 18(1), 89-110.
- [16] List, C., & Puppe, C. (2009). Judgment aggregation: A survey. In P. Anand, P. Pattanaik, & C. Puppe (Eds.), *Handbook of Rational and Social Choice* (pp. 457-482). Oxford University Press.
- [17] Fishburn, P. C. (1970). Arrow's impossibility theorem: Concise proof and infinite voters. *Journal of Economic Theory*, 2(1), 103-106.
- [18] Kirman, A. P., & Sondermann, D. (1972). Arrow's theorem, many agents, and invisible dictators. *Journal of Economic Theory*, 5(2), 267-277.
- [19] Lauwers, L., & Van Liedekerke, L. (1995). Ultraproducts and aggregation. *Journal of Mathematical Economics*, 24(3), 217-237.
- [20] Mallows, C. L. (1957). Non-null ranking models. I. *Biometrika*, 44(1/2), 114-130.
- [21] Lu, T., & Boutilier, C. (2011). Learning Mallows models with pairwise preferences. *Proceedings of the 28th International Conference on Machine Learning*, 145-152.
- [22] Black, D. (1948). On the rationale of group decision-making. *Journal of Political Economy*, 56(1), 23-34.
- [23] Bubenik, P., & Scott, J. A. (2015). Categorification of persistent homology. *Discrete & Computational Geometry*, 51(3), 600-627.